

Lev Truskinovsky · Anna Vainchtein

## Beyond kinetic relations

Received: 21 October 2009 / Accepted: 20 May 2010 / Published online: 3 September 2010  
© Springer-Verlag 2010

**Abstract** We introduce the concept of *kinetic or rate equations* for moving defects representing a natural extension of the more conventional notion of a *kinetic relation*. Algebraic kinetic relations, widely used to model dynamics of dislocations, cracks and phase boundaries, link the instantaneous value of the velocity of a defect with an instantaneous value of the driving force. The new approach generalizes kinetic relations by implying a relation between the velocity and the driving force which is nonlocal in time. To make this relation explicit one may need to integrate a system of kinetic equations. We illustrate the difference between kinetic relation and kinetic equations by working out in full detail a prototypical model of an overdamped defect in a one-dimensional discrete lattice. We show that the minimal nonlocal kinetic description, containing now an internal time scale, is furnished by a system of two ordinary differential equations coupling the spatial location of defect with another internal parameter that describes configuration of the core region.

**Keywords** Martensitic phase transitions · Lattice dynamics · Kinetic relations · Kinks · Defects · Quasicontinuum models · Dispersion · Nonlinear waves

### 1 Introduction

Kinetic relations attributing a particular value of velocity to a given value of the driving force are widely used in continuum mechanics as a constitutive description of moving lattice defects including phase boundaries, dislocations, and cracks (see the reviews [2, 16, 28, 30]). These algebraic relations form independent postulates that serve as closing conditions specifying singular solutions in the classical continuum theories. Kinetic relations replace the detailed modeling of the core regions of the defects and represent a condensed description of the complex physical behavior at the microscale. In practice, kinetic relations are either taken from experiment or deduced from the solutions of auxiliary microscale problems. Characteristically, these auxiliary problems always assume constant values of both the macroscopic velocity of the defect and of the corresponding driving force.

Due to the implicit assumption that the defect is in a steady motion, the kinetic relations based description misses the details of a non-steady internal dynamics of the core region. In particular, the internal pulsations originating from the defect interaction with localized micro-inhomogeneities become averaged out. To partially

---

Communicated by Stefan Seelecke.

L. Truskinovsky  
Laboratoire de Mécanique des Solides, CNRS-UMR 7649, Ecole Polytechnique, 91128 Palaiseau, France  
E-mail: trusk@lms.polytechnique.fr

A. Vainchtein (✉)  
Department of Mathematics, University of Pittsburgh, Pittsburgh, PA 15260, USA  
E-mail: aav4@pitt.edu

recover the missing information we propose in this paper to replace algebraic kinetic relations by differential *kinetic equations*. The aim of these equations is to capture the transient phases of the defect evolution in response to non-steady driving.

In the language of constitutive theory, we propose to replace the instantaneous rheological relations for moving defects by nonlocal memory functionals originating from a local description in terms of internal variables. Such augmentation of the model brings into the conventional theory internal time scales and allows one to deal with the so-called “rate effects”. An example of a similar development is provided by the rate-dependent constitutive laws in the theory of friction, where the set of internal state variables is also assumed to satisfy differential constitutive relations (e.g. [32,33]).

In order to show the possibility of a systematic derivation of kinetic equations from a micromodel, we consider a prototypical overdamped defect moving in a lattice. We develop a low-parametric description of the internal dynamics of this defect involving some specially selected internal variables which characterize the structure of the core region. Our approach can be viewed as an example of a quasicontinuum method in the sense of [4,29,37] because we match the macroscopic continuum description outside singularities with a more detailed atomistic resolution of the core regions. The zero-order model of this type produces kinetic relations and implies instantaneous and universal response of the core region to external perturbations (autonomous core region). The first-order approximation leads to kinetic equations which capture some non-universal features of the microscopic dynamics. For consistency of the two approximations, kinetic equations must of course reduce to the kinetic relation when the variation of the macroscopic parameters is sufficiently slow.

In this paper, we illustrate the general idea of our approach to kinetics by considering the case of a martensitic phase transition. Phase boundaries are particularly convenient for the demonstration of our main principles because these plane defects can be adequately represented already in one-dimensional models. To emphasize ideas we limit our attention to overdamped dynamics. At the microscale, the analysis of the non-steady evolution of the transformation front requires a study of a dynamical system with an infinite number of degrees of freedom. At the macroscale, the phase transition is modeled as a singular surface (jump discontinuity) whose evolution is governed by a kinetic relation [38]. We pose the question of whether an intermediate description is possible when the interface is equipped with a small number of “mesoscopic” degrees of freedom whose dynamics reproduces the main transient effects.

Probably the first example of such a reduced description can be found in the theory of lattice dislocations where a dynamic defect is often viewed as an effective particle moving in the Peierls–Nabarro (PN) landscape [7]. The PN landscape is obtained by relaxing all microscopic variables other than one collective variable interpreted as the macroscopically observable location of the core. The idea of a tilted PN landscape has been heuristically applied to the description of dynamic dislocations in close to continuum limit [13,17–20,27,31,45]. This approach, however, cannot be used in principle in the strongly discrete case when the dislocation core is atomically narrow [14,21]. In order to deal with this limit, it is natural to abandon the idea of macroscopic collective variables and trace instead the dynamics of the particular discrete elements while enslaving all others. Such elements were called “localized normal modes” in [44] and “active points” in [24]. In some special cases it can be proven rigorously that dynamics of “active points” corresponds to the motion along the center manifold of the infinite-dimensional dynamical system [9].

In the absence of a systematic approach, the internal variables capturing the main response of a defect to a particular class of external perturbations have to be chosen heuristically. In this paper, we propose to base the selection of the minimal set of relevant parameters on the analysis of the relative “activity” of the variables in the traveling wave solution. As a result, we obtain kinetic equations which describe small (and adiabatic) modulations of such steady states. Stronger deviations from the traveling wave ansatz have been rigorously studied for several classes of nonlinear equations in the case of periodic obstacles (pulsating traveling fronts, e.g., [5,11]). Here we deal with singular limit of such problems (localization of the fronts) which has not been fully understood in the mathematical literature.

The paper is organized as follows. To show the limitations of the algebraic kinetic relations and to motivate the ideas behind the construction of the differential kinetic equations, we begin in Sect. 2 with a toy model. In Sect. 3, we formulate the singular macroscopic problem which requires a closure relation. We then discuss different phenomenological options, including local and nonlocal kinetic relations. In search for a more physically sound microscopic closure we turn in Sect. 4 to a lattice model of a moving defect. The kinetic equations of different dimensionality are proposed in Sect. 5. By studying the exact traveling wave solution of our discrete problem, which is known in the case of a piecewise quadratic interaction potential [36,42,43], we conclude in Sect. 6 that the system of kinetic equations must be at least two-dimensional. In Sect. 7, we test our low-parametric reduced model in the case of a time-dependent driving force and show how it can be

used to obtain a rheological model of the transformation kinetics which is nonlocal in time. We also show that depending on the rate of external driving the responses of the phase boundary based on the kinetic relation and on the associated kinetic equations may be markedly different. Our conclusions are summarized in Sect. 8. Explicit traveling wave solution of the microscopic problem which is used in the paper as a benchmark test is constructed in Appendix A. In Appendix B, we show that at least for adiabatic variations of the driving force the system of kinetic equations inherits the gradient flow structure from the microscopic model.

## 2 Motivation

To motivate our approach, we begin with a toy model describing an overdamped dynamics of a configurational point in a one-dimensional energy landscape:

$$\frac{\partial v}{\partial \tau} = -\frac{\partial \Phi(v; G(t))}{\partial v}. \quad (1)$$

Here  $v$  is a variable defining the microstate of the system and  $G(t)$  is a sufficiently slow varying macroscopic driving force which depends on slow time  $t$ . The fast time is defined as  $\tau = t/\epsilon$ , where  $\epsilon \ll 1$  is a small parameter. We assume that the gradient of the energy landscape  $\Phi(v; G)$  is periodic in  $v$ . For example, one can consider (see also [3])

$$\Phi(v; G) = G_P \delta \sin \frac{v}{\delta} - Gv, \quad (2)$$

where the parameter  $\delta > 0$  measures the degree of discreteness of the system, which is manifested here through the “wiggles” in the energy landscape. Thus,  $\delta \rightarrow 0$  represents the continuum limit, while  $\delta \sim 1$  is the strongly discrete regime. The Peierls driving force  $G_P > 0$  is a depinning threshold: at  $|G| < G_P$  the system is trapped in one of the local minima of the energy landscape, which become saddle points at  $G = \pm G_P$ ; at  $|G| > G_P$  the configurational point starts moving.

The method of kinetic relations postulates the existence of an algebraic relation between the driving force  $G$  and the macroscopic velocity

$$V(t) = \left\langle \frac{\partial v}{\partial \tau} \right\rangle_\tau = \lim_{\epsilon \rightarrow 0} \epsilon \int_0^{1/\epsilon} \frac{\partial v}{\partial \tau} d\tau. \quad (3)$$

Such relation, which we write as  $V(t) = \mathcal{F}(G(t))$ , can be computed explicitly if  $\Phi(v; G)$  is given by (2). Then (e.g. [3, 15])

$$V = \Gamma(G) = \begin{cases} 0 & |G| \leq G_P \\ \text{sgn}(G - G_P) \sqrt{G^2 - G_P^2} & |G| \geq G_P. \end{cases} \quad (4)$$

In more realistic situations, the microscopic description of the type (1) is too complex because it involves a huge number of variables. In contrast, the macroscopic description (4) is too schematic and cannot be trusted when one deals with the problems where slow and fast time scales cannot be separated. Consider, for instance, time-dependent driving force given by

$$G(t) = G_0 - A \tanh \frac{t - t_*}{\zeta}. \quad (5)$$

Here  $G_0 = G(t_*) > G_P$  is the constant background driving force,  $A$  is the amplitude of the (diffuse) jump in the driving force, and  $\zeta$  is the characteristic time over which the driving force decreases by  $2A$ . Such perturbation of the driving force may represent an interaction of a dislocation or a phase boundary with an obstacle.

Compare two responses to the perturbation (5). One is obtained by solving the *kinetic equation*

$$\frac{\partial v}{\partial t} = G(t) - G_P \cos \frac{v}{\delta} \quad (6)$$

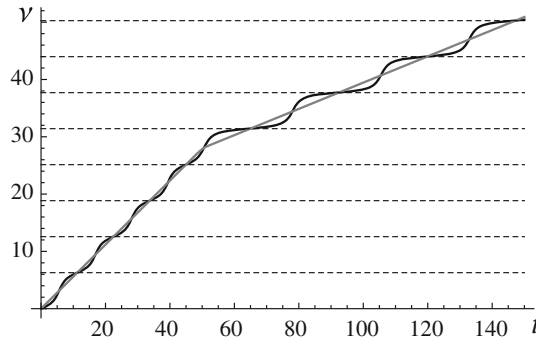


**Fig. 1** The transient response in the model (2) to a time-dependent variation of the driving force (5) with  $A = 0.1$ ,  $t_* = 50$ ,  $G_0 = 0.65$  and  $\zeta = 1$ ,  $G_P = 0.5$  and  $\delta = 1$ . The curves  $v(t)$  (black curve) and  $v_*(t)$  (gray curve) are obtained using (6) and (7), respectively. Horizontal dashed lines indicate the discrete locations  $2\pi n\delta$  of the lattice points

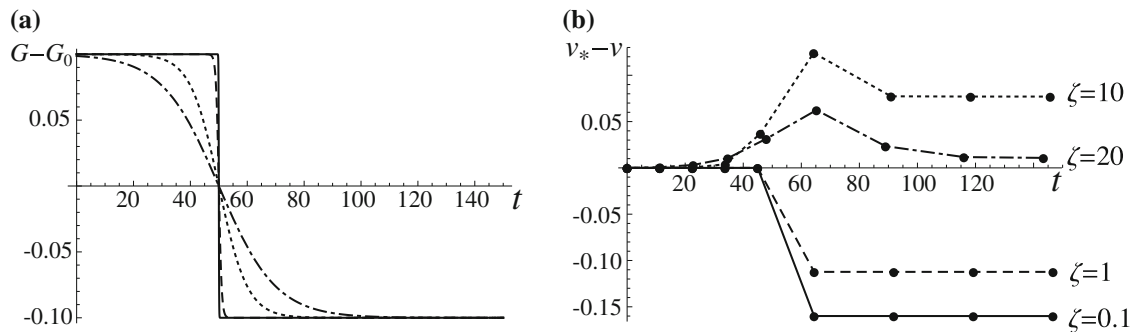


**Fig. 2 a** Time-dependent driving force (5) with  $A = 0.1$ ,  $t_* = 50$ ,  $G_0 = 0.65$  and different  $\zeta$  in the model (2) with  $G_P = 0.5$  and  $\delta = 1$ . **b** The corresponding difference  $v_*(t) - v(t)$  evaluated at the times  $t_n$  when  $v(t_n) = 2\pi n\delta$

for  $v(t)$ . The other response is governed by the kinetic relation (4) at  $G > G_P$  and is given by

$$v_*(t) = \int_0^t \mathcal{F}(G(\tau)) d\tau = \int_0^t \sqrt{G^2(\tau) - G_P^2} d\tau. \tag{7}$$

Typical results are shown in Fig. 1. One can see that as  $G(t)$  decreases, the average velocity decreases, resulting in the smaller slope of both graphs. Observe also that while the parameter  $v$  changes continuously with time  $t$ , the core of the moving defect modeled by this system can take values at the discrete lattice points  $2\pi n\delta$  (the inflection points of  $\Phi(v; G_P)$ ) shown by dashed lines in Fig. 1b. The difference  $v_*(t) - v(t)$  at the times  $t_n$  when  $v(t_n) = 2\pi n\delta$  is shown in Fig. 2b for different values of  $\zeta$  (with the corresponding  $G(t)$  graphs shown in part (a)). One can see that for each  $\zeta$  the difference is nearly zero at  $t$  small enough so that  $G(t)$  is almost constant, becomes nonzero as  $G(t)$  decreases and tends to a constant nonzero value at large  $t$ . The large difference between the two responses at small  $\zeta$  indicates that kinetic relation approach is not suitable when  $G(t)$  changes sufficiently fast. As  $\zeta$  becomes larger, the difference between the two responses tends to zero, suggesting that kinetic relation approach produces adequate approximation above a certain threshold in  $\zeta$ .

To understand how this threshold depends on the inhomogeneity level without solving the time-dependent problem, one can consider a constant  $G > G_P$  and replace the driving rate  $\zeta$  by the size of the observation window. Introduce an auxiliary function

$$\tau(q, \delta, G) = \delta \int_0^q \frac{dp}{G - G_P \cos p} = 2\delta \frac{\arctan \left[ \frac{\sqrt{G^2 - G_P^2}}{G - G_P} \tan \frac{q}{2} \right] + \pi \left[ \frac{q + \pi}{2\pi} \right]}{\sqrt{G^2 - G_P^2}},$$

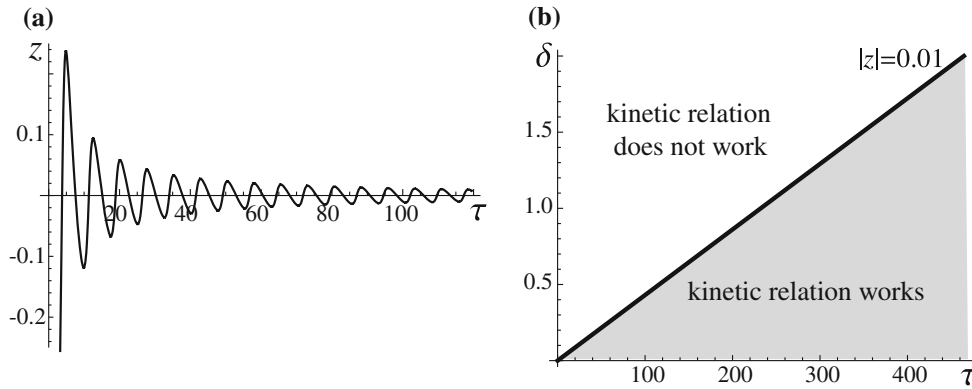


**Fig. 3** **a** The misfit  $z$  between the coarse-grained and the kinetic relation based descriptions vs the size of the averaging window  $\tau$  at  $\delta = 0.5$ . **b** The threshold  $|z| = 0.01$  separating the region in  $\delta - \tau$  plane where the kinetic relation approach is suitable from the region where kinetic relation can not be expected to work well. Here  $G = 0.65$

where  $q > 0$ , and  $\lfloor x \rfloor$  denotes the largest integer less or equal than  $x$ . We can now define a coarse-grained velocity

$$V_c(q, G) = \frac{q\delta}{\tau(q, \delta, G)}.$$

The quantity

$$z(q, G) = \frac{V_c(q, G)}{\mathcal{F}(G)} - 1,$$

which is independent of  $\delta$ , quantifies the error of the approximation of the coarse-grained velocity  $V_c(q, G)$  by the kinetic relation (4). The parametric plot of  $z(q, G)$  versus  $\tau(q, \delta, G)$  at  $\delta = 0.5$  and  $G = 0.65$  is shown in Fig. 3a. One can see that this is an oscillating function that decreases in amplitude as the window  $\tau$  decreases. Therefore, kinetic relation approach becomes justified only when  $\tau$  is sufficiently large. Using the threshold value  $|z| = 0.01$  we find that the domain in the  $(\tau, \delta)$  plane where kinetic relation works is bounded by a linear function representing the critical scaling (see Fig. 3b). The existence of such a crossover indicates, in particular, that the continuum limit  $\delta \rightarrow 0$  is nonuniform with respect to  $\tau$ .

### 3 Macroscopic model

Let  $u(x, t)$  be a one-dimensional continuum displacement field. The macroscopic energy of a bar undergoing martensitic phase transition can be written as

$$\mathcal{E} = \int \left[ \frac{\rho u_t^2}{2} + \phi(u_x) \right] dx. \quad (8)$$

Here  $u_t \equiv \partial u / \partial t$  is the macroscopic velocity,  $u_x \equiv \partial u / \partial x$  is the macroscopic strain,  $\rho > 0$  is the reference mass density, and the energy density  $\phi(u_x)$  is represented by a double-well potential which will be specified later.

The dynamic equation corresponding to the energy (8) is

$$\rho u_{tt} = (\hat{\sigma}(u_x))_x, \quad (9)$$

where  $\hat{\sigma}(u_x) = \phi'(u_x)$  is the stress-strain relation. On discontinuities, the Eq. 9 must be supplemented with the jump conditions. Let  $f_-$  and  $f_+$  denote the values of  $f(x)$  to the left and to the right of the interface, and introduce the notations  $\llbracket f \rrbracket \equiv f_+ - f_-$  for the jump and  $\{f\} \equiv (f_+ + f_-)/2$  for the average of  $f$  across the discontinuity. Then the parameters on a discontinuity must satisfy the classical Rankine-Hugoniot jump conditions

$$\llbracket u_t \rrbracket + V \llbracket u_x \rrbracket = 0, \quad \rho V \llbracket u_t \rrbracket + \llbracket \hat{\sigma}(u_x) \rrbracket = 0. \quad (10)$$

The entropy inequality, which must also hold on the jump, can be written in the form

$$\mathcal{R} = GV \geq 0, \quad (11)$$

where  $\mathcal{R}$  is the rate of energy dissipation and

$$G = \llbracket \phi \rrbracket - \{\hat{\sigma}(u_x)\} \llbracket u_x \rrbracket \quad (12)$$

is the configurational (driving) force. In one-dimensional problems, imposing the entropy inequality can remedy local non-uniqueness only in the case of supersonic discontinuities (shock waves). For subsonic phase boundaries one must specify the rate of entropy production as well. This is usually done phenomenologically through the kinetic relation  $V = \mathcal{F}(G)$  linking the driving force and the velocity [1, 38, 39]. If the microscopic model is known, one can compute the function  $\mathcal{F}(V)$  directly from the microscopic traveling wave solution (e.g. [34, 36, 38, 42, 43]).

Since the adjustment of the velocity  $V(t)$  to the dynamic configurational loading  $G(t)$  is not instantaneous, the algebraic kinetic relation cannot be expected to work well if the function  $G(t)$  changes sufficiently fast. In this case, the more realistic relationship between the velocity and the driving force will be history-dependent:

$$V(t) = \mathcal{F}\{G(\tau), \tau \leq t\}. \quad (13)$$

The goal of the following sections is to find the way such a nonlocal relationship can be reconstructed from a microscopic model and to show that the nonlocality may be important in the case of nonadiabatic driving.

For simplicity, we limit our attention in what follows to the overdamped limit. In this case, the macroscale governing equations (9) reduce to

$$(\hat{\sigma}(u_x))_x = 0.$$

The Rankine–Hugoniot jump conditions take the form

$$\llbracket \hat{\sigma}(u_x) \rrbracket = 0.$$

Suppose now that the overdamped dynamics of the transformation front can be described on the microscale by a system of equations in the form

$$\dot{\mathbf{w}} = \mathcal{R}(\mathbf{w}; G(t)), \quad (14)$$

where  $G(t)$  is the macroscopic driving force (12) entering the microscopic equations as a time-dependent parameter. If we could solve these equations and express the velocity of the transformation front through the micro-parameters  $\mathbf{w} \in \mathbb{R}^N$ , the problem of reconstructing the nonlocal kinetic relation (13) would be solved. In view of the large value of  $N$  this is hardly possible. Therefore, we can try to approximate the higher-dimensional dynamical system (14) by a low-dimensional dynamical system of the type

$$\dot{\mathbf{v}} = \mathcal{Q}(\mathbf{v}; G(t)), \quad (15)$$

where now  $\mathbf{v} \in \mathbb{R}^K$  and  $K \ll N$  defines the dimensionality of the reduced system. After the solution of the vector Eq. 15 is known, the microscopic discrete field (14) should be recoverable from the auxiliary relations  $w_n(t) = w_n(v_1(t), \dots, v_K(t))$  describing the “non-order-parameter” variables. The knowledge of the dynamics of the front in terms of the variables  $\mathbf{v}$  will then be sufficient for finding the nonlocal relation between the front velocity  $V(t)$  and the driving  $G(t)$ .

Observe that behind the conventional assumption that there exists an algebraic relation between the driving force,  $G$ , and the velocity,  $V$ , lies the idea that the width of the transition layer is so small that the internal relaxation to the traveling wave profile takes place much faster than the variation of the driving force. However, as we have seen in our toy example, the convergence to the sharp interface limit may be nonuniform with respect to the parameter describing the rate of configurational loading. This becomes important if, for instance, our phase boundary interacts with an obstacle. The structure of this obstacle should be sufficiently diffuse for the algebraic kinetic relation to hold. If the profile of the obstacle is sufficiently sharp, the time scales of internal relaxation and of external driving may become comparable and the traveling wave ansatz may break. In this case, one can expect that more complex double limits in the spirit of [6] may still work and we view our kinetic equations as a step towards constructing such intermediate asymptotics.

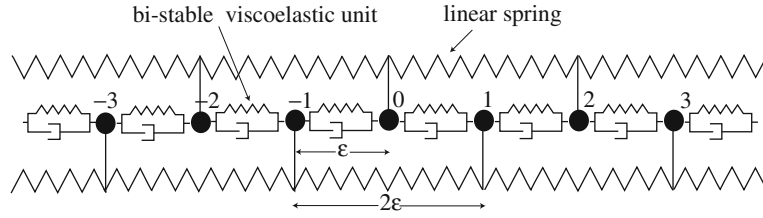


**Fig. 4** The discrete microstructure with viscoelastic nearest and elastic next-to-nearest-neighbor interactions

#### 4 Microscopic model

Consider an infinite chain of particles, connected to their nearest neighbors (NN) through viscoelastic springs and to their next-to-nearest neighbors (NNN) by elastic springs (see Fig. 4).

Suppose that in the undeformed configuration the NN and NNN springs have lengths  $\varepsilon$  and  $2\varepsilon$ , respectively. Let  $u_n(t)$  denote the displacement of  $n$ th particle at time  $t$  with respect to the reference configuration. We associate with the deformation of  $n$ th NN spring a discrete measure of strain

$$w_n = \frac{u_n - u_{n-1}}{\varepsilon}. \quad (16)$$

For the viscoelastic NN springs we assume the following constitutive relation:

$$f_{\text{NN}}(w, \dot{w}) = \phi'_{\text{NN}}(w) + \xi \dot{w}, \quad (17)$$

where  $\xi > 0$  is the viscosity coefficient. To describe domain boundaries the function  $\phi_{\text{NN}}(w)$  must be at least a double-well potential; to simplify the analysis we also assume that this function is biquadratic:

$$\phi_{\text{NN}}(w) = \begin{cases} \frac{1}{2}\mu w^2, & w \leq w_c \\ \frac{1}{2}\mu(w-a)^2 + \mu a(w_c - \frac{a}{2}), & w \geq w_c. \end{cases} \quad (18)$$

Under these assumptions the NN elastic units can be in two different phases, depending on whether the strain is below (phase I) or above (phase II) the critical value  $w_c$ . The elastic modulus in each phase is  $\mu > 0$ , and the parameter  $a > 0$  measures the transformation strain. To further simplify calculations, we assume that the NNN interactions are linearly elastic:

$$f_{\text{NNN}}(\hat{w}) = 2\gamma \hat{w}. \quad (19)$$

Here we defined  $\hat{w}_n = (w_{n+1} + w_n)/2$  as the strain in the NNN spring connecting  $(n+1)$ th and  $(n-1)$ th particles.

The dynamics of the chain is governed by the following system of ordinary differential equations:

$$\begin{aligned} \rho \varepsilon \ddot{u}_n = & \mu[w_{n+1} - w_n - \theta(w_{n+1} - w_c)a + \theta(w_n - w_c)a] \\ & + \gamma(w_{n+2} + w_{n+1} - w_n - w_{n-1}) + \xi(\dot{w}_{n+1} - \dot{w}_n). \end{aligned} \quad (20)$$

Here  $\rho > 0$  is the mass density of the chain and  $\theta(x)$  is the unit step function. To ensure stability of the chain we require that

$$E = \mu + 4\gamma > 0, \quad (21)$$

where  $E$  is the homogenized macroscopic elastic modulus; following [40,41], we also assume that the NNN interactions are of ferromagnetic type, meaning that  $\gamma \leq 0$ . In the limit  $\varepsilon/L \rightarrow 0$ , where  $L$  is a macroscopic length scale, the viscosity term tends to zero and we recover (9) with the homogenized stress–strain law [43]

$$\hat{\sigma}(w) = E(w - \Delta\theta(w - w_c)).$$

Here  $\Delta$  is the macroscopic transformation strain:

$$\Delta = \frac{a\mu}{E}. \quad (22)$$

There are two time scales associated with this problem: the time scale of inertia,  $T_{\text{in}} = \varepsilon\sqrt{\rho/E}$ , and the viscosity time scale,  $T_{\text{visc}} = \xi/E$ . In what follows we limit our attention to the overdamped limit when  $T_{\text{visc}} \gg T_{\text{in}}$ , i.e.

$$\xi \gg \varepsilon\sqrt{\rho E}. \quad (23)$$

We can then nondimensionalize the problem using  $T_{\text{visc}}$  as the time scale and letting

$$\bar{t} = \frac{tE}{\xi}, \quad \bar{u}_n = \frac{u_n}{\Delta\varepsilon}, \quad \bar{w}_n = \frac{w_n}{\Delta}, \quad \bar{w}_c = \frac{w_c}{\Delta}. \quad (24)$$

Dropping the bars on the new variables, we obtain dimensionless system equations:

$$\dot{w}_n - \dot{w}_{n+1} = \hat{\sigma}(w_{n+1}) - \hat{\sigma}(w_n) + D(w_{n+2} - 3w_{n+1} + 3w_n - w_{n-1}), \quad (25)$$

where

$$\hat{\sigma}(w) = w - \theta(w - w_c) \quad (26)$$

is the rescaled macroscopic stress–strain law. The dimensionless parameter

$$D = -\frac{\gamma}{E} \geq 0 \quad (27)$$

characterizes the relative strength of NN and NNN interactions. In what follows it will also be interpreted as a measure of coupling of the bistable units.

Observe that system (25) can be “integrated”, yielding

$$\dot{w}_n = D(w_{n+1} - 2w_n + w_{n-1}) - \hat{\sigma}(w_n) + \sigma. \quad (28)$$

Here  $\sigma = \sigma(t)$  is the time-dependent applied stress. One can see that we obtained the overdamped Frenkel–Kontorova (FK) model [9, 12, 23, 26]. A subtle but important particularity of the present setting is that in contrast to the usual setting of the FK model our coupling coefficient  $D$  is independent of the spatial scale  $\varepsilon$ .

## 5 Kinetic equations

To obtain a reduced model, we seek to condense out all but a small number of strain variables governing the evolution of the core region of the moving phase boundary. The key to our approach will be the assumption that the dynamics of only a few bonds located in the core region has to be resolved fully. A careful study of the traveling wave solution of the infinite-dimensional system (28) presented in the Appendix A shows that other bonds remain confined to near bottoms of their respective potential wells, and their small adjustment to the changing conditions can be treated as instantaneous. In a certain sense we extend the approach of “active points” [9, 24] introduced first to deal with the immediate vicinity of the depinning point to a broader class of non-steady motions.

We start by choosing a single active point and follow its exact dynamics while instantaneously equilibrating all other microstrain variables at a current value of the driving force  $G(t)$ . More specifically, we assume that dynamics of only a single NN spring, located right behind the phase transition front and actually changing the energy well, needs to be traced in all the detail, while all other springs can be “enslaved” to it.

We can always assume that at  $t = 0$  it is the 0th NN spring that has just switched from phase I to phase II and therefore, the “active strain” is  $w_0$  and  $w_0(0) = w_c$ . The other strain variables  $w_n$ ,  $n \neq 0$ , satisfy the system of equilibrium equations

$$D(w_{n+1} - 2w_n + w_{n-1}) - \hat{\sigma}(w_n) + \sigma = 0, \quad (29)$$

where  $n \neq 0$ . Since we deal with an isolated phase boundary, we assume that at infinity the solution of (29) approaches uniform-strain  $G$ -dependent states in two different phases:

$$\lim_{k \rightarrow -\infty} w_k = G + w_c + 1/2, \quad \lim_{k \rightarrow \infty} w_k = G + w_c - 1/2. \quad (30)$$

Introducing

$$\lambda = \operatorname{arccosh}\left(\frac{1}{2D} + 1\right), \quad (31)$$

we obtain

$$w_n = w_c - 1/2 + G + \begin{cases} 1 + (w_0 - w_c - G - 1/2)e^{\lambda n}, & n \leq -1 \\ (w_0 - w_c - G + 1/2)e^{-\lambda n}, & n \geq 1, \end{cases} \quad (32)$$

which also extends to  $n = 0$ . Substituting these expressions in (28) with  $n = 0$ , we obtain a single equation governing the dynamics of the active point:

$$\dot{w}_0 = -w_0\{1 + 2D(1 - e^{-\lambda})\} + w_c + G + 1/2 + 2D(G + w_c)(1 - e^{-\lambda}). \quad (33)$$

Equation 33 is the simplest example of a differential *kinetic equation* generalizing the algebraic *kinetic relation* (47).

To obtain a more sophisticated reduced model which can be expected to work in a wider range of driving conditions, we need to incorporate more “active points” into the monitored core region of the defect. The natural next step is to consider in addition to  $w_0(t)$  the adjacent strains  $w_{-1}(t)$ , and  $w_1(t)$ . We therefore assume again that  $G = \text{const}$  and equilibrate all strain variables other than  $w_{-1}$ ,  $w_0$  and  $w_1$ . This leads to the following recovery relations:

$$w_n = \begin{cases} w_c + G + 1/2 + (w_{-1} - w_c - G - 1/2)e^{\lambda(n+1)}, & n \leq -1 \\ w_0, & n = 0 \\ w_c + G - 1/2 + (w_1 - w_c - G + 1/2)e^{\lambda(1-n)}, & n \geq 1. \end{cases} \quad (34)$$

The three active variables satisfy the dynamic equations

$$\begin{aligned} \dot{w}_{-1} &= D(w_0 - 2w_{-1} + w_{-2}) - w_{-1} + w_c + G + 1/2 \\ \dot{w}_0 &= D(w_1 - 2w_0 + w_{-1}) - w_0 + w_c + G + 1/2 \\ \dot{w}_1 &= D(w_2 - 2w_1 + w_0) - w_1 + w_c + G - 1/2. \end{aligned} \quad (35)$$

Substituting the expressions for  $w_2$  and  $w_{-2}$  from (34) in (36), we obtain

$$\begin{aligned} \dot{w}_{-1} &= (-2D - 1 + e^{-\lambda}D)w_{-1} + Dw_0 + (w_c + G + 1/2)(1 + D(1 - e^{-\lambda})) \\ \dot{w}_0 &= (-2D - 1)w_0 + Dw_1 + Dw_{-1} + w_c + G + 1/2 \\ \dot{w}_1 &= (-2D - 1 + e^{-\lambda}D)w_{-1} + Dw_0 + (w_c + G - 1/2)(1 + D(1 - e^{-\lambda})). \end{aligned} \quad (36)$$

If we now compare the equations governing the dynamics of  $w_{-1}(t)$  and  $w_1(t)$ , we see that they differ only by a constant term. This allows us to reduce (37) to a two-dimensional system for

$$x(t) = w_0(t), \quad y(t) = \frac{w_{-1}(t) + w_1(t)}{2}. \quad (37)$$

These two variables,  $x(t)$ , describing the dynamics of the transforming spring, and  $y(t)$ , describing the average strain in the core region, must satisfy the following system of equations:

$$\begin{aligned} \dot{x} &= (-2D - 1)x + 2Dy + w_c + G + 1/2 \\ \dot{y} &= Dx + (-2D - 1 + e^{-\lambda}D)y + (w_c + G)(1 + D(1 - e^{-\lambda})). \end{aligned} \quad (38)$$

This system of *kinetic equations* generalizes (33) and will serve in what follows as our main approximation of the full microscopic dynamics. Note that the active strains can be recovered from (38), (39) by means of explicit formulas:  $w_{\mp 1}(t) = y(t) \pm (1 - e^{-\lambda})/2$ . The described process of extracting higher and higher order systems of kinetic equations can be of course continued until one recovers the original infinite-dimensional system.

Note that at  $t = t_1$ , when  $w_1(t_1) = w_c$  the core region moves by one lattice space, and the equations governing the reduced models need to be modified accordingly. In general, during the time interval  $t_i \leq t < t_{i+1}$ , where  $t_i$  is such that  $w_i(t_i) = w_c$ , the active strains are  $w_i$  and (in  $K = 2$  case)  $w_{i\pm 1}$ .

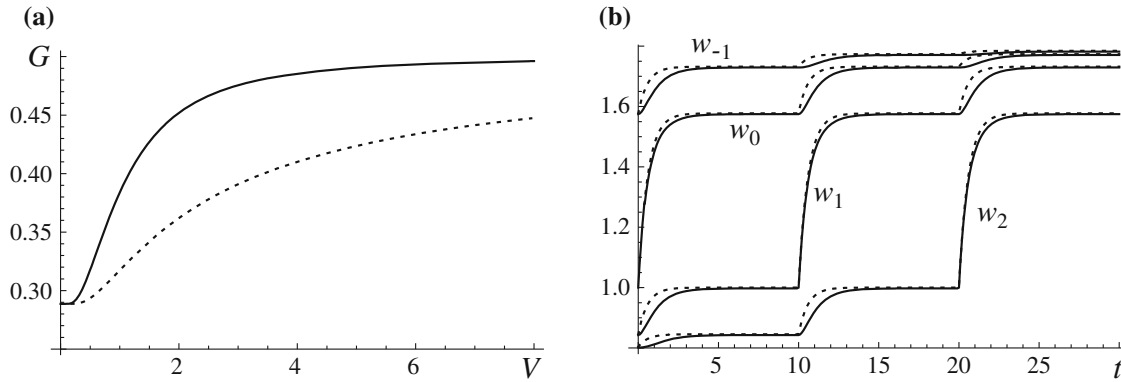


**Fig. 5** **a** Kinetic relations  $G(V)$  for the infinite-dimensional dynamics (64) (solid curve) and for the  $K = 1$  approximation (dotted curve). **b** Comparison of strain trajectories obtained in the  $K = 1$  reduced model (dotted curves) and in the original infinite-dimensional model (solid curves). Parameters:  $V = 0.1$ ,  $D = 0.5$ ,  $w_c = 1$

## 6 Kinetic relation

To show the advantage of the two-dimensional system (38), (39) over the one-dimensional equation (33), we consider in this section the simplest steady-state regime with  $G(t) = \text{const}$  and  $w_n(t) = w(n - Vt)$ . The corresponding solution of the infinite-dimensional problem describing a steadily propagating phase boundary is known explicitly (see Appendix A).

To see whether the simplest kinetic equation with  $K = 1$  is compatible with the exact kinetic relation (64), we solve (33) subject to the boundary condition  $w_0(0) = w_c$ , obtaining

$$w_0(t) = w_c + (G + G_P) \left\{ 1 - \exp\left(-\frac{t}{2G_P}\right) \right\}. \quad (40)$$

Here  $G_P$  is the classical Peierls threshold introduced in the Appendix A (see (67)). Next, by setting  $n = 1$  in (32), we find

$$w_1(t) = w_c + G - G_P - e^{-\lambda}(G + G_P) \exp\left(-\frac{t}{2G_P}\right).$$

The second boundary condition  $w_1(1/V) = w_c$  yields the desired approximation of the kinetic relation:

$$G(V) = G_P + \frac{(1 - e^{-\lambda})(G_S - G_P)}{\exp\left(\frac{1}{2G_P V}\right) - \exp(-\lambda)}. \quad (41)$$

Clearly,  $G(V) \rightarrow G_P$  as  $V \rightarrow 0$ , and in agreement with (64)  $G(V)$  tends to the spinodal value  $G_S = 1/2$  as  $V$  goes to infinity.

In Fig. 5b, we compare the dynamics governed by the one-dimensional model (33) with the full infinite-dimensional dynamics at  $G = \text{const}$  which follows from the traveling wave solution (62). As expected, the evolution of the active strain is captured quite well, but there is a visible deviation from the actual values for the strains whose adjustment was assumed to be instantaneous. The corresponding kinetic relations are compared in Fig. 5a. One can see that the reduced model with  $K = 1$  provides a good quantitative approximation of the exact kinetic relation until  $V = 0.2$ . At higher velocities it deviates substantially from the exact relation, although both tend to the same spinodal limit  $G_S$  at infinite  $V$ . The observed discrepancies in the case  $G = \text{const}$  suggest that the reduced model with  $K = 1$  may be oversimplified.

We now turn to the kinetic equations with  $K = 2$  and check whether the traveling wave solution (62) of the original system can be reproduced by the reduced system (38), (39). Such solution must be subjected to a set of constraints. First, we must require that

$$x(0) = w_c, \quad (42)$$

a condition that ensures that the 0th NN spring (recall that  $x = w_0$ ) has just transformed to the new phase at  $t = 0$ . Second, we require that

$$w_1(1/V) = w_c,$$

or

$$y(1/V) = w_c + \frac{1 - e^{-\lambda}}{2}. \quad (43)$$

This means that at  $t = 1/V$  the first NN spring reaches the critical strain, marking the end of the first time interval. Finally, the traveling wave ansatz requires that

$$w_1(0) = w_2(1/V).$$

Using (34) at  $n = 2$  together with (43), we can see that this boundary condition reduces to

$$w_1(0) = w_c - (G_S - G)(1 - e^{-\lambda}),$$

or

$$y(0) = w_c + G(1 - e^{-\lambda}). \quad (44)$$

Next, by solving the system (38), (39) subject to the initial conditions (42) and (44), we obtain

$$\begin{aligned} x(t) &= w_c + G + G_P + c_1 e^{r_1 t} + c_2 e^{r_2 t} \\ y(t) &= w_c + G + e^{-\lambda} G_P + \frac{e^{-\lambda}}{4} (c_1 (1 + \sqrt{1 + 8e^{2\lambda}}) e^{r_1 t} + c_2 (1 - \sqrt{1 + 8e^{2\lambda}}) e^{r_2 t}), \end{aligned} \quad (45)$$

where

$$r_{1,2} = -\frac{e^\lambda}{4 \sinh^2(\lambda/2)} \left( 1 + \frac{1}{2} e^{-2\lambda} (1 \mp \sqrt{1 + 8e^{2\lambda}}) \right) \quad (46)$$

(note that  $r_2 < r_1 < 0$ ) and

$$\begin{aligned} c_1 &= -\frac{(3 + \sqrt{1 + 8e^{2\lambda}})(2G - 1 + e^\lambda(1 + 2G))}{4(1 + e^\lambda)\sqrt{1 + 8e^{2\lambda}}} \\ c_2 &= -\frac{(\sqrt{1 + 8e^{2\lambda}} - 3)(2G - 1 + e^\lambda(1 + 2G))}{4(1 + e^\lambda)\sqrt{1 + 8e^{2\lambda}}}. \end{aligned}$$

The application of the boundary condition (43) yields the following approximation of the kinetic relation:

$$G(V) = \frac{G_P + \frac{1 - e^{-\lambda}}{4(1 + e^\lambda)\sqrt{1 + 8e^{2\lambda}}} \left( (1 + 2e^{2\lambda} + \sqrt{1 + 8e^{2\lambda}}) e^{r_1/V} + (\sqrt{1 + 8e^{2\lambda}} - 2e^{2\lambda} - 1) e^{r_2/V} \right)}{1 - \frac{e^{-\lambda}}{2\sqrt{1 + 8e^{2\lambda}}} \left( (1 + 2e^{2\lambda} + \sqrt{1 + 8e^{2\lambda}}) e^{r_1/V} + (\sqrt{1 + 8e^{2\lambda}} - 2e^{2\lambda} - 1) e^{r_2/V} \right)}. \quad (47)$$

Notice again that the approximate kinetic relation (47) satisfies the constraint  $G(0) = G_P$ . Then, as  $V$  tends to infinity,  $G(V) \rightarrow G_S = 1/2$ . The global comparison of the approximate and exact kinetic relations is presented in Fig. 6a. One can see that in view of how few degrees of freedom are involved in the approximation (two), the agreement is quite good.

The comparison of strain trajectories in the two-dimensional reduced theory with the exact result at  $G = \text{const}$  shows a considerable improvement over the one-dimensional approximation. For instance, Fig. 6b compares the evolution of strains near the phase boundary over the first three time intervals at  $V = 0.1$ . While in the case  $K = 1$  the evolution of only the transforming element could be followed closely over each time interval, in the  $K = 2$  case the dynamics of the all nontransforming elements forming the core region of the defect is also captured extremely well.

In Fig. 7, we show the regions in the  $(D, V)$  plane where the reduced models capture the exact kinetics within 1% error. The errors are defined as follows:

$$e_{1,2}(V, D) = |1 - G_{1,2}(V, D)/G_{\text{ex}}(V, D)|,$$

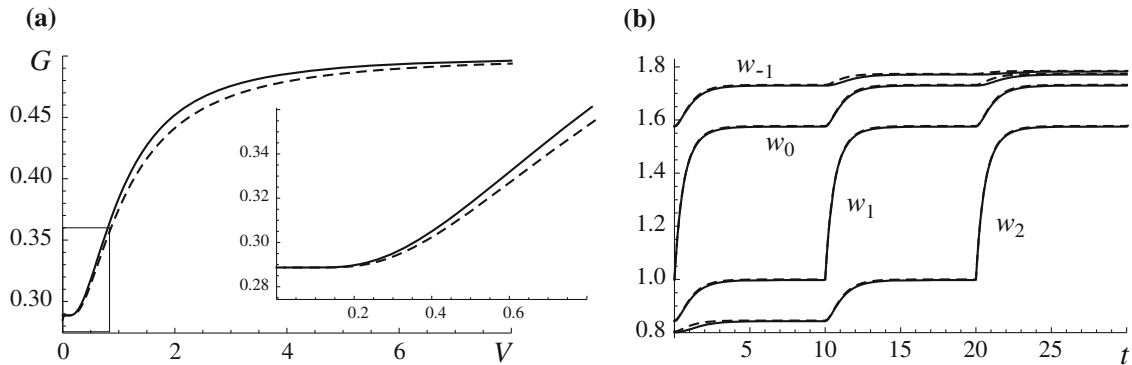


**Fig. 6** **a** Kinetic relations  $G(V)$ : infinite-dimensional system (64) (solid curve) and  $K = 2$  approximation (dashed curve); **b** Comparison of the strain trajectories obtained in the  $K = 2$  model (dashed curves) and in the infinite-dimensional model (solid curves). Parameters:  $V = 0.1$ ,  $D = 0.5$ ,  $w_c = 1$

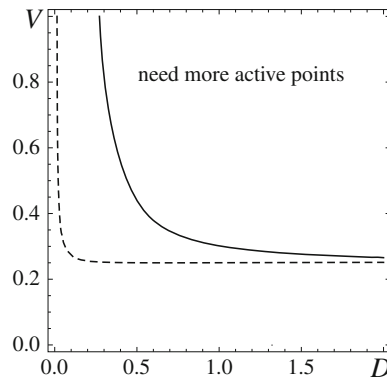


**Fig. 7** The boundaries of the region in the  $(D, V)$  plane where the errors  $e_1(V, D)$  (dashed line) and  $e_2(V, D)$  (solid line) in the approximation of the exact kinetic relation by  $K = 1$  and  $K = 2$  reduced models, respectively, are less than 1%

where  $G_1(V, D)$ ,  $G_2(V, D)$ , and  $G_{\text{ex}}(V; D)$  are given by (41), (47) and (64), respectively. One can see that at  $V < 0.25$  both approximations are within this error margin for all  $D$ . The error becomes much smaller as  $V$  decreases (e.g. less than 0.002% error for  $K = 2$  approximation at  $V = 0.1$ ). At higher velocities the agreement is good only for small enough  $D$  (strongly discrete limit, narrow core), with the threshold value of  $D$  depending on  $V$ . At larger  $D$  (strong coupling limit, broad core) the transformation front delocalizes and more and more active points need to be included (see also [9]).<sup>1</sup>

In summary, we have shown that the kinetic model with  $K = 2$  performs well in a much larger parameter range than the kinetic model with  $K = 1$ . It is then natural to use the  $K = 2$  system as the basis for the construction of the nonlocal rheological relation on the moving phase boundary. An interpretation of the  $K = 2$  dynamics as the overdamped motion of an effective configurational particle in a two-dimensional dynamic Peierls–Nabarro energy landscape is discussed in Appendix B.

## 7 Nonsteady dynamics

We saw that the traveling wave solution of the original infinite-dimensional system can be reproduced rather faithfully by the reduced two-dimensional system (38) and (39). This suggests that the  $K = 2$  model may be extended to deal with the situation when the driving force is not constant but varies sufficiently slowly. In this more general setting we obtain

$$\begin{aligned} \dot{x} &= (-2D - 1)x + 2Dy + w_c + G(t) + 1/2 \\ \dot{y} &= Dx + (-2D - 1 + e^{-\lambda}D)y + (w_c + G(t))(1 + D(1 - e^{-\lambda})). \end{aligned} \quad (48)$$

<sup>1</sup> Another possibility is to change the type of the approximation from “active points” to “collective variables”, which is more in tune with a close to continuum character of the model in this limit. We will not pursue these ideas in the present paper.

The system of kinetic equations (48) introduces an implicit nonlocal kinetic relation  $V(t) = \mathcal{F}\{G(\tau), \tau \leq t\}$ .

To reconstruct this nonlocal relation we first suppose that the phase boundary is located at  $n = i$  at time  $t = t_i$ , meaning that in this instance the  $i$ th spring has critical strain:  $w_i(t_i) = w_c$ . As before, we can define  $x(t) = w_i(t)$  and  $y(t) = (w_{i+1}(t) + w_{i-1}(t))/2$  when  $t_i \leq t < t_{i+1}$ . Our goal is to compute the average velocity  $\bar{V}_i$  in the interval  $(t_i, t_{i+1})$ , under the assumption that  $G(t)$  is known.

Observe that conditions

$$x(t_i) = w_c \quad (49)$$

and

$$y(t_{i+1}) = w_c + \frac{1 - e^{-\lambda}}{2}, \quad (50)$$

which are the extensions of (42) and (43) to the interval  $[t_i, t_{i+1})$ , ensure that the system holds from  $t = t_i$  until the time  $t_{i+1}$  when the next spring reaches the critical strain:  $w_{i+1}(t_{i+1}) = w_c$ . While for given  $t_{i+1}$  conditions (49) and (50) are sufficient to find a unique solution of (48), the moment  $t_{i+1}$  when the consecutive spring switches from one energy well to another remains unknown. If  $G(t)$  varies sufficiently slowly, it is reasonable to assume that the motion is close to steady in the sense that<sup>2</sup>

$$w_i(t_i) = w_{i+1}(t_{i+1}). \quad (51)$$

This condition allows us to close the system and find  $t_{i+1}$  from

$$y(t_i) = w_c + G(t_{i+1})(1 - e^{-\lambda}). \quad (52)$$

To this end, we solve (48) subject to (49) and (52), obtain for  $t_i \leq t \leq t_{i+1}$ ,

$$\begin{aligned} x(t) &= g(t) + \int_{t_i}^t (e^{r_1(t-\tau)} f_1(\tau) + e^{r_2(t-\tau)} f_2(\tau)) d\tau \\ y(t) &= h(t) + \frac{e^{-\lambda}}{4} \int_{t_i}^t \left\{ (1 + \sqrt{1 + 8e^{2\lambda}}) e^{r_1(t-\tau)} f_1(\tau) \right. \\ &\quad \left. + (1 - \sqrt{1 + 8e^{2\lambda}}) e^{r_2(t-\tau)} f_2(\tau) \right\} d\tau, \end{aligned} \quad (53)$$

where we defined

$$\begin{aligned} g(t) &= \frac{1}{\sqrt{1 + 8e^{2\lambda}}} \left\{ \frac{1}{2} \left( (\sqrt{1 + 8e^{2\lambda}} - 1) e^{r_1(t-t_i)} + (\sqrt{1 + 8e^{2\lambda}} + 1) e^{r_2(t-t_i)} \right) w_c \right. \\ &\quad \left. + 2e^\lambda (e^{r_1(t-t_i)} - e^{r_2(t-t_i)}) (w_c + G(t_{i+1})(1 - e^{-\lambda})) \right\} \\ h(t) &= \frac{1}{\sqrt{1 + 8e^{2\lambda}}} \left\{ e^\lambda (e^{r_1(t-t_i)} - e^{r_2(t-t_i)}) w_c \right. \\ &\quad \left. + \frac{1}{2} \left( (\sqrt{1 + 8e^{2\lambda}} + 1) e^{r_1(t-t_i)} + (\sqrt{1 + 8e^{2\lambda}} - 1) e^{r_2(t-t_i)} \right) (w_c + G(t_{i+1})(1 - e^{-\lambda})) \right\} \quad (54) \\ f_1(t) &= \frac{\sqrt{1 + 8e^{2\lambda}} - 1}{2\sqrt{1 + 8e^{2\lambda}}} \left( w_c + \frac{1}{2} + G(t) \right) + \frac{2e^\lambda}{\sqrt{1 + 8e^{2\lambda}}} (w_c + G(t))(1 + D(1 - e^{-\lambda})) \\ f_2(t) &= \frac{\sqrt{1 + 8e^{2\lambda}} + 1}{2\sqrt{1 + 8e^{2\lambda}}} \left( w_c + \frac{1}{2} + G(t) \right) - \frac{2e^\lambda}{\sqrt{1 + 8e^{2\lambda}}} (w_c + G(t))(1 + D(1 - e^{-\lambda})). \end{aligned}$$

<sup>2</sup> This condition is obviously not exact because  $G(t_i) \neq G(t_{i+1})$ . By using the knowledge of the exact structure of the traveling waves at both  $G(t_i)$  and  $G(t_{i+1})$  this approximation can be in principle improved.

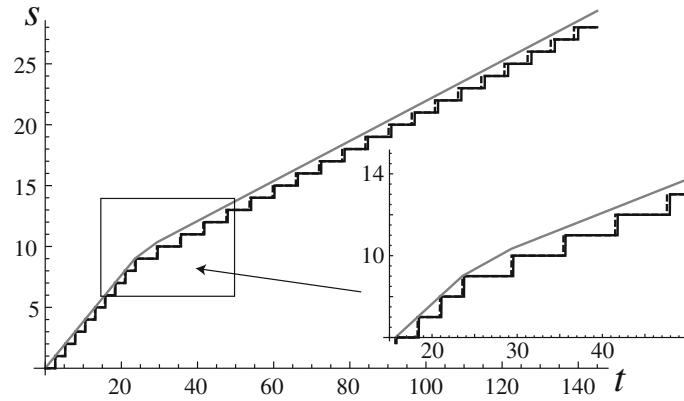


**Fig. 8** Position  $s(t)$  of the phase boundary obtained from the numerical solution of the discrete system (28) on a truncated lattice (black solid curve), kinetic equations (48) (dashed line) and kinetic relation (47) for the reduced  $K = 2$  model (gray curve) under time-dependent driving force (5). Here  $D = 0.1$ ,  $G_0 = 0.4295$ ,  $A = 0.0065$ ,  $\zeta = 1$ , and  $t_* = 25$

We can now determine the strains  $w_i(t) = x(t)$  and  $w_{i\mp 1}(t) = y(t) \pm (1 - e^{-\lambda})/2$ . The other strains can be recovered as before, from the constrained energy minimization:

$$w_n(t) = \begin{cases} w_c + G(t) + 1/2 + (w_{i-1} - w_c - G(t) - 1/2)e^{\lambda(n-i+1)}, & n \leq i - 2 \\ w_c + G(t) - 1/2 + (w_{i+1} - w_c - G(t) + 1/2)e^{\lambda(1-n-i)}, & n \geq i + 2. \end{cases}$$

Condition (50) applied to  $y(t)$  in (53) yields the nonlinear equation for  $t_{i+1}$ :

$$h(t_{i+1}) - w_c - \frac{1 - e^{-\lambda}}{2} + \frac{e^{-\lambda}}{4} \int_{t_i}^{t_{i+1}} \left\{ (1 + \sqrt{1 + 8e^{2\lambda}})e^{r_1(t_{i+1}-\tau)} f_1(\tau) + (1 - \sqrt{1 + 8e^{2\lambda}})e^{r_2(t_{i+1}-\tau)} f_2(\tau) \right\} d\tau = 0. \quad (55)$$

As we have seen in the previous section, at  $G = \text{const}$  this equation has a unique solution and one can expect that at least for the case of slowly varying driving force  $G(t)$  the solution  $t_{i+1}$  also exists and is unique. Once it is found, we can obtain the desired expression for the average velocity in the time interval  $(t_i, t_{i+1})$ :

$$\bar{V}_i = \frac{1}{t_{i+1} - t_i}. \quad (56)$$

Using this iterative process, one can generate the sequence of successive time intervals  $[t_i, t_{i+1}]$  and the piecewise constant function

$$s(t) = i, \quad t_i \leq t < t_{i+1}$$

describing the position of the phase boundary according to the reduced model. To illustrate this procedure, consider the time-dependent driving force (5) with  $G_0 = 0.4295$ ,  $A = 0.0065$ ,  $\zeta = 1$  and  $t_* = 25$  and let  $D = 0.1$ . In Fig. 8, we see the dynamics  $s(t)$  of the phase boundary responding to this loading if computed from (48) with  $s(0) = 0$  (dashed curve). It is compared to the dynamic trajectory generated numerically by solving the original discrete system (28) (black solid curve) on a truncated lattice (600 lattice points) with initial strain given by the traveling wave solution at  $G = G(0)$  that has one of the springs at the critical strain  $w_c$ . In both cases the front initially propagates with a steady speed corresponding to constant driving force  $G(t) \approx G_0 + A$ . As the driving force decreases at  $22 \leq t \leq 28$  (see the curve  $\zeta = 1$  in Fig. 9), there is a transient regime followed, for  $t > 28$ , by another nearly steady regime at a lower velocity corresponding to the lower value  $G(t) \approx G_0 - A$ . One can see that there is a delay in the response of the original system with respect to the reduced one due to the approximations we made to obtain and solve (48).

Figure 8 also compares the two history-dependent trajectories of the front with the corresponding instantaneous response obtained from the kinetic relation (47) (gray curve). In this case, we obtain  $V_*(t) = \mathcal{F}(G(t))$

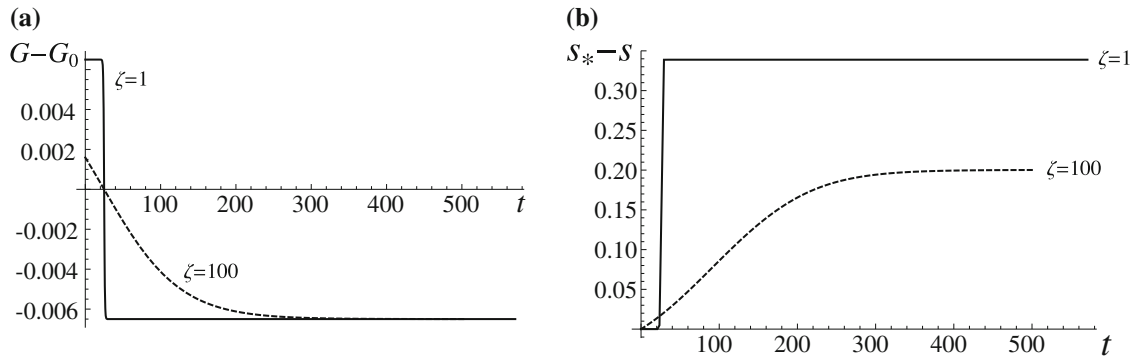


**Fig. 9** **a** Time-dependent driving force (5), with  $\zeta = 1$  (solid curve) and  $\zeta = 100$  (dashed curve). **b** The corresponding difference between the coordinate  $s_*(t)$  of the phase boundary obtained using the instantaneous kinetic response  $V(t) = \mathcal{F}(G(t))$  and the coordinate  $s(t)$  calculated using the kinetic equations (48). Here  $D = 0.1$ ,  $G_0 = 0.4295$ ,  $A = 0.0065$  and  $t_* = 25$

by inverting (47), and the location  $s_*(t)$  of the phase boundary assuming  $s_*(0) = 0$  can be found by integration from

$$s_*(t) = \int_0^t \mathcal{F}(G(\tau)) d\tau.$$

Initially, all three responses are close but as driving force decreases, the phase boundary location obtained using the kinetic relation is found to be ahead of the history-dependent responses of the full and reduced discrete systems. This is seen more clearly in Fig. 9, which shows the difference  $s_*(t) - s(t)$  between the front locations found using the kinetic relation (47) and the kinetic equation (48). The comparison is made at the discrete moments of time  $t_i$  obtained in the iterative procedure described above. As in the zero-dimensional toy model presented in Sect. 2 the two kinetic models converge and the difference  $s_*(t) - s(t)$  tends to zero as  $\zeta \rightarrow \infty$ . However, as Fig. 9 shows, at finite  $\zeta$  the prediction of the model based on the local *kinetic relation* may be markedly different from the one obtained by solving the system of *kinetic equations*.

## 8 Conclusions

In the classical macroscopic continuum description of lattice defects the core regions are represented by singularities, and the dynamics of these singularities is governed by algebraic kinetic relations. Such description is too coarse to capture the details of the dynamic response of the cores of the defects to relatively fast changes of the macroscopic driving forces. It also averages out the details of the intricate interaction of the core regions with localized micro-inhomogeneities which manifests itself through microscopic velocity oscillations and leads to macroscopically observable acoustic emission. We can refer, for instance, to scale-free acoustic emission accompanying plasticity, martensitic phase transitions, and fracture (e.g. [22]).

To describe the “breathing” of the core regions as well as other transient effects that are usually neglected, we proposed in this paper to replace the algebraic relations between the macroscopic velocity and the corresponding driving force, which imply internal steady state, by a system of differential kinetic equations. The explicit time dependence of the driving force makes these equations nonautonomous and allows them to capture the nonlocal relation between the current value of velocity and the history of the driving force. Therefore, the ensuing rheological description of the moving defect can be qualified as a *differential rate model*.

The main idea of our construction is to follow the exact dynamics of only few discrete degrees of freedom. Minimizing out the infinite number of the remaining variables outside the core region serves as the matching condition with the classical continuum description outside the defect. The choice of the dimensionality of the reduced system remains heuristic and is based on the comparison of steady solutions of the finite-dimensional system with the discrete traveling wave solutions of the microscopic infinite-dimensional model. We show that in contrast to the standard approach that involves only the center of mass of the defect, the minimally adequate approximation includes not only the location but also the internal configuration of the core. Such extension of the scope is necessary even if both the *macroscopic* driving force and the average velocity of the defect are

constant because the core region can experience *microscopic* configurational deformations rather than being translated as a rigid body.

In this paper, we presented only the contours of the nonlocal approach to kinetic relations and provided only the most elementary illustrations. More rigorous study is necessary to formulate a systematic center-manifold-type reduction procedure and to evaluate the errors of the finite-dimensional approximation of kinetics in mathematical terms. Other problems include transition from overdamped to underdamped dynamics and generalization to higher dimensions. Special development is also needed to advance from a prototypical case of a martensitic phase boundary to the geometrically more challenging cases of dislocations, cracks, and point singularities.

**Acknowledgements** This work was supported by the US National Science Foundation grant DMS-0443928 (A.V.) and by the EU contract MRTN-CT-2004-505226 (L.T.).

## 9 Appendix

### A Traveling wave solution and its static limit

To construct a traveling wave solution of the system (28) with  $\sigma = \text{const}$ , we assume that

$$w_n(t) = w(\eta), \quad \eta = n - Vt, \quad (57)$$

where  $V$  is the dimensionless velocity of the front, which represents a moving phase boundary. Since we seek a description of an isolated phase boundary that leaves phase II behind, we require that

$$w(\eta) < w_c \quad \text{for } \eta > 0, \quad w(\eta) > w_c \quad \text{for } \eta < 0 \quad (58)$$

Under these assumptions, (28) reduces to

$$V w'(\eta) - D(w(\eta + 1) - 2w(\eta) + w(\eta - 1)) + w(\eta) = \theta(-\eta) + \sigma. \quad (59)$$

At infinity the solution must tend to uniform-strain equilibria of (25):

$$w(\eta) \rightarrow w_{\pm} \quad \text{as } \eta \rightarrow \pm\infty. \quad (60)$$

Finally, for consistency, we must also require that

$$w(0) = w_c. \quad (61)$$

The Eq. 59 is linear in each phase, and it can be solved using Fourier transform (see [9, 12, 43] for details). We obtain

$$w(\eta) = \begin{cases} \sigma + 1 + \sum_{k \in S^-(V)} \frac{e^{ik\eta}}{k\Lambda_k(k, V)} & \text{for } \eta < 0 \\ \sigma - \sum_{k \in S^+(V)} \frac{e^{ik\eta}}{k\Lambda_k(k, V)} & \text{for } \eta > 0, \end{cases} \quad (62)$$

where  $S^{\pm}(V) = \{k : \Lambda(k, V) = 0, \text{Im}k \gtrless 0\}$  are the sets of roots of the dispersion relation

$$\Lambda(k, V) \equiv 1 + 4D \sin^2(k/2) - Vik = 0.$$

Continuity of  $w(\eta)$  at  $\eta = 0$  gives the relationship between the applied stress and velocity of the traveling wave:

$$\sigma = \sigma_M + \frac{1}{2} + \sum_{k \in S^+(V)} \frac{1}{k\Lambda_k(k, V)} = \sigma_M - \frac{1}{2} - \sum_{k \in S^-(V)} \frac{1}{k\Lambda_k(k, V)}, \quad (63)$$

where  $\sigma_M = w_c - 1/2$  is the Maxwell stress. Since the difference between applied and Maxwell stresses is equal to the driving force  $G = \sigma - \sigma_M$  (see [42]), we obtain the *kinetic relation* between the driving force and the velocity of the moving front:

$$G(V) = \frac{1}{2} + \sum_{k \in \mathcal{S}^+(V)} \frac{1}{k \Lambda_k(k, V)}. \quad (64)$$

This semianalytic expression remains implicit until one finds the exact locations of the roots  $k = k(V)$  of the dispersion equation (see [43]).

In the static limit ( $V = 0$ ) the continuous variable  $\eta = n - Vt$  takes discrete values, and the strain profile becomes discontinuous at every integer  $\eta$ . The differential equation reduces to a system of finite-difference equations, and we can replace the continuous Fourier transform by its discrete analog [42] (see also [10, 25, 35]). Both this procedure and the direct solution of the difference equations, yield the following family of stationary solutions [12, 17, 40]:

$$w_n^m(G) = \sigma_M + \begin{cases} G + 1 - \frac{\exp(\lambda(n - m - 1/2))}{2 \cosh(\lambda/2)}, & n < m \\ G + \frac{\exp(-\lambda(n - m - 1/2))}{2 \cosh(\lambda/2)}, & n \geq m, \end{cases} \quad (65)$$

with the phase boundary located at  $n = m$ . The admissibility constraints

$$w_n^m \geq w_c \quad \text{for } n \leq m, \quad w_n^m \leq w_c \quad \text{for } n \geq m + 1 \quad (66)$$

determine the constraints on  $G$ ; the set of driving forces satisfying these constraints constitutes the *trapping region*. One can show that in the present case of repulsive long-range interactions ( $D > 0$ ) the strain profile (65) is monotone, so the constraints (66) can be replaced by  $w_m^m \geq w_c$  and  $w_{m+1}^m \leq w_c$ . The trapping region is then given by  $|G| \leq G_P$ , where

$$G_P = \frac{1}{2\sqrt{1+4D}} = \frac{1}{2} \tanh \frac{\lambda}{2} \quad (67)$$

is the *Peierls force* (see also [8, 40]). The phase boundary remains trapped until the driving force reaches one of the limiting values:  $G = -G_P$ , when the interface starts moving to the left ( $V < 0$ ), or  $G = G_P$ , when the interface starts moving to the right ( $V > 0$ ). The two limiting solutions represent unstable equilibria from which the dynamic solution bifurcates.

## B Dynamic Peierls–Nabarro landscape

In the overdamped limit the microscopic equation (28) can be rewritten in the gradient-flow form

$$\dot{\mathbf{w}} = -\nabla \mathcal{W}(\mathbf{w}; G(t)). \quad (68)$$

Here  $\mathbf{w} \in \mathbb{R}^\infty$  is the vector of strains, the gradient is taken with respect to  $\mathbf{w}$ , and

$$\mathcal{W} = \sum_{n=-\infty}^{\infty} \left( \frac{1}{2} w_n^2 - (w_n - w_c) \theta(w_n - w_c) + \frac{1}{2} D (w_{n+1} - w_n)^2 - (\sigma_M + G(t)) w_n \right) \quad (69)$$

is the dimensionless energy of the system. It is natural to ask whether the reduced dynamics can also be expressed as a gradient flow in a particular potential. With this potential we associate our dynamic Peierls–Nabarro (PN) landscape.

In view of what has been found in Sect. 6 we need to focus on the case  $K = 2$ . We shall also assume that the landscape is evolving slowly in the time scale of internal dynamics so that we can use adiabatic approximation and assume that  $G = \text{const}$ .

We recall that expressions (45), (37), and (34) define the strain trajectories  $w_n(t)$  only over the time interval  $0 \leq t \leq 1/V$ . The desired extension of this solution for  $k/V \leq t \leq (k+1)/V$  can be obtained by replacing  $n$  in the above formulas by  $n - k$  and  $t$  by  $t - k/V$ . To patch together different intervals we need to introduce a set of two order parameters that change continuously and monotonically with  $t$ .

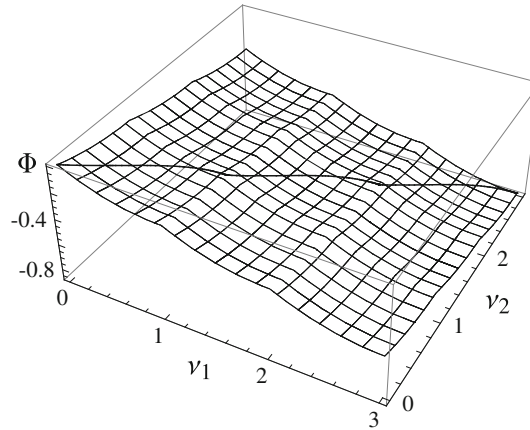


**Fig. 10** Two-dimensional dynamic PN energy landscape  $\Phi(v_1, v_2)$  and the path of the effective particle  $\mathbf{v}(t)$ . Parameters:  $V = 0.1$ ,  $D = 0.5$ ,  $w_c = 1$

Observe first that in (46) we have  $|r_2| > |r_1| > 0$ , so that the eigenvector  $(\frac{e^{-\lambda}}{4}(\sqrt{1+8e^{2\lambda}}+1), 1)$  corresponding the eigenvalue  $r_2$  is the slow direction, while the eigenvector  $(\frac{e^{-\lambda}}{4}(1-\sqrt{1+8e^{2\lambda}}), 1)$  that corresponds to  $r_1$  is the fast direction. Introduce the *slow* variable

$$v_1(t) = \lfloor Vt \rfloor + \frac{1 - \exp(r_1(t - \lfloor Vt \rfloor / V))}{1 - \exp(r_1 / V)} \quad (70)$$

and the *fast* variable

$$v_2(t) = \lfloor Vt \rfloor + \frac{1 - \exp(r_2(t - \lfloor Vt \rfloor / V))}{1 - \exp(r_2 / V)}. \quad (71)$$

In terms of the new variables, the time evolution of all strains is given by

$$w_n(t) = \begin{cases} w_c + G + 1/2 + \{G_P - 1/2 + \frac{1}{4}c_1(1 + \sqrt{1+8e^{2\lambda}})(1 - (1 - e^{r_1/V})(v_1(t) - \lfloor Vt \rfloor)) \\ + c_2(1 - \sqrt{1+8e^{2\lambda}})(1 - (1 - e^{r_2/V})(v_2(t) - \lfloor Vt \rfloor))\}e^{\lambda(n - \lfloor Vt \rfloor)}, & n \leq \lfloor Vt \rfloor - 1 \\ w_c + G + G_P + c_1(1 - (1 - e^{r_1/V})(v_1(t) - \lfloor Vt \rfloor)) \\ + c_2(1 - (1 - e^{r_2/V})(v_2(t) - \lfloor Vt \rfloor)), & n = \lfloor Vt \rfloor \\ w_c + G - 1/2 + \{G_P + 1/2 + \frac{1}{4}c_1(1 + \sqrt{1+8e^{2\lambda}})(1 - (1 - e^{r_1/V})(v_1(t) - \lfloor Vt \rfloor)) \\ + c_2(1 - \sqrt{1+8e^{2\lambda}})(1 - (1 - e^{r_2/V})(v_2(t) - \lfloor Vt \rfloor))\}e^{-\lambda(n - \lfloor Vt \rfloor)}, & n \geq \lfloor Vt \rfloor + 1. \end{cases} \quad (72)$$

The vector field  $\mathbf{v}(t) = (v_1(t), v_2(t))$  satisfies

$$\dot{\mathbf{v}} = -\alpha \nabla \Phi(\mathbf{v}; G), \quad (73)$$

where the mobility matrix  $\alpha = \text{diag}(\alpha_1, \alpha_2)$  is diagonal (here  $\alpha_1 > 0$  and  $\alpha_2 > 0$  are constants). The dynamic PN potential  $\Phi(v_1, v_2; G)$  is piecewise quadratic; it depends on  $V$  and hence, through the kinetic relation  $V = \mathcal{F}(G)$  given by (47), on the driving force  $G$ . Using (70) and (71), we obtain

$$\Phi(v_1, v_2; G) = -\frac{r_1}{2\alpha_1} \left\{ (v_1 - \lfloor v_1 \rfloor)^2 - \frac{2}{1 - \exp(r_1/\mathcal{F}(G))} v_1 + \lfloor v_1 \rfloor \right\} \\ - \frac{r_2}{2\alpha_2} \left\{ (v_2 - \lfloor v_2 \rfloor)^2 - \frac{2}{1 - \exp(r_2/\mathcal{F}(G))} v_2 + \lfloor v_2 \rfloor \right\}.$$

To determine the effective viscosities  $\alpha_1$  and  $\alpha_2$ , we require that at  $G = G_P$  the dynamic PN potential equals the relative Gibbs free energy of the system:

$$\Phi(\mathbf{v}; G_P) = \mathcal{W}(\mathbf{w}(\mathbf{v}); G_P) - \mathcal{W}(\mathbf{w}(\mathbf{0}); G_P).$$

This yields

$$\alpha_1 = -\frac{r_1\sqrt{1+8e^{2\lambda}}}{(\sqrt{1+8e^{2\lambda}}+3)G_P}, \quad \alpha_2 = -\frac{r_1\sqrt{1+8e^{2\lambda}}}{(\sqrt{1+8e^{2\lambda}}-3)G_P} \quad (74)$$

and, finally,

$$\begin{aligned} \Phi(v_1, v_2; G) = & \frac{(\sqrt{1+8e^{2\lambda}}+3)G_P}{2\sqrt{1+8e^{2\lambda}}} \left\{ (v_1 - \lfloor v_1 \rfloor)^2 - \frac{2}{1 - \exp(r_1/\mathcal{F}(G))} v_1 + \lfloor v_1 \rfloor \right\} \\ & + \frac{(\sqrt{1+8e^{2\lambda}}-3)G_P}{2\sqrt{1+8e^{2\lambda}}} \left\{ (v_2 - \lfloor v_2 \rfloor)^2 - \frac{2}{1 - \exp(r_2/\mathcal{F}(G))} v_2 + \lfloor v_2 \rfloor \right\}. \end{aligned} \quad (75)$$

The dynamic PN landscape  $\Phi(v_1, v_2; G)$ , along with the trajectory of the effective particle, is shown in Fig. 10.

## References

1. Abeyaratne, R., Knowles, J.: Kinetic relations and the propagation of phase boundaries in solids. *Arch. Ration. Mech. Anal.* **114**, 119–154 (1991)
2. Abeyaratne, R., Knowles, J.K.: *Evolution of Phase Transitions, A Continuum Theory*. Cambridge University Press, London (2006)
3. Abeyaratne, R., Chu, C., James, R.D.: Kinetics of materials with wiggly energies: theory and application to the evolution of twinning microstructures in a Cu-Al-Ni shape memory alloy. *Phil. Mag. A* **73**, 457–497 (1996)
4. Arndt, M., Luskin, M.: Error estimation and atomistic-continuum adaptivity for the quasicontinuum approximation of Frenkel-Kontorova model. *Multiscale Model. Simul.* **7**, 147–170 (2008)
5. Berestycki, H., Hamel, F.: Front propagation in periodic excitable media. *Commun. Pure Appl. Math.* **55**, 949–1032 (2002)
6. Braides, A., Truskinovsky, L.: Asymptotic expansions by  $\Gamma$ -convergence. *Continuum Mech. Thermodyn.* **20**(1), 21–62 (2008)
7. Braun, O.M., Kivshar, Y.S.: *The Frenkel-Kontorova Model: Concepts, Methods And Applications*. Texts and Monographs in Physics. Springer-Verlag, Berlin, Heidelberg (2004)
8. Braun, O.M., Kivshar, Y.S., Zelenskaya, I.I.: Kinks in the Frenkel-Kontorova model with long-range interparticle interactions. *Phys. Rev. B* **41**, 7118–7138 (1990)
9. Carpio, A., Bonilla, L.L.: Depinning transitions in discrete reaction-diffusion equations. *SIAM J. Appl. Math.* **63**(3), 1056–1082 (2003)
10. Celli, V., Flytzanis, N.: Motion of a screw dislocation in a crystal. *J. Appl. Phys.* **41**(11), 4443–4447 (1970)
11. Dirr, N., Yip, N.K.: Pinning and depinning phenomena in front propagation in heterogeneous media. *Interfaces Free Boundaries* **8**, 79–109 (2006)
12. F ath, G.: Propagation failure of traveling waves in discrete bistable medium. *Physica D* **116**, 176–190 (1998)
13. Flach, S., Kladko, K.: Perturbation analysis of weakly discrete kinks. *Phys. Rev. E* **54**, 2912–2916 (1996)
14. Furuya, K., de Almeida, A.M.O.: Soliton energies in the standard map beyond the chaotic threshold. *J. Phys. A* **20**, 6211–6221 (1987)
15. Gruner, G., Zawadowski, A., Chaikin, P.M.: Nonlinear conductivity and noise due to charge-density-wave depinning in NbSe<sub>3</sub>. *Phys. Rev. Lett.* **46**, 511–515 (1981)
16. Gurtin, M.E.: *Configurational Forces as Basic Concepts of Continuum Physics*. Applied Mathematical Sciences, vol. 137. Springer-Verlag, New York (1999)
17. Hobart, R.: Peierls stress dependence on dislocation width. *J. Appl. Phys.* **36**, 1944–1948 (1965)
18. Hobart, R.: Peierls barrier analysis. *J. Appl. Phys.* **37**, 3573–3576 (1966)
19. Ishibashi, Y., Suzuki, I.: On the evaluation of the pinning (Peierls) energy of kinks due to discreteness of substrate lattices. *J. Phys. Soc. Jpn.* **53**, 4250–4256 (1984)
20. Ishimori, Y., Munakata, T.: Kink dynamics in the discrete Sine-Gordon system: a perturbational approach. *J. Phys. Soc. Jpn.* **51**, 3367–3374 (1982)
21. Joos, B.: Properties of solitons in the Frenkel-Kontorova model. *Solid State Commun.* **42**, 709–713 (1982)
22. Kardar, M.: Nonequilibrium dynamics of interfaces and lines. *Phys. Rep.* **301**, 85–112 (1998)
23. Keener, J.P.: Propagation and its failure in coupled systems of discrete excitable cells. *SIAM J. Appl. Math.* **47**(3), 556–572 (1987)
24. Kladko, K., Mitkov, I., Bishop, A.R.: Universal scaling of wave propagation failure in arrays of coupled nonlinear cells. *Phys. Rev. Lett.* **84**(19), 4505–4508 (2000)
25. Kresse, O., Truskinovsky, L.: Mobility of lattice defects: discrete and continuum approaches. *J. Mech. Phys. Solids* **51**, 1305–1332 (2003)
26. Kresse, O., Truskinovsky, L.: Prototypical lattice model of a moving defect: the role of environmental viscosity. *Izvestiya, Phys. Solid Earth* **43**, 63–66 (2007)
27. Lazutkin, V.F., Schachmannski, I.G., Tabanov, M.B.: Splitting of separatrices for standard and semistandard mappings. *Physica D* **40**, 235–348 (1989)
28. LeFloch, P.G.: *Hyperbolic Systems of Conservation Laws*. ETH Lecture Note Series. Birkhuser, Switzerland (2002)
29. Li, X., E, W.: Multiscale modeling of the dynamics of solids at finite temperature. *J. Mech. Phys. Solids* **53**, 1650–1685 (2005)

30. Maugin, G.A.: *Material Inhomogeneities in Elasticity*. Applied Mathematics and Mathematical Computation: vol 3. Chapman and Hall, London (1993)
31. Pokrovsky, V.L.: Splitting of commensurate-incommensurate phase transition. *J. Phys. (Paris)* **42**(6), 761–766 (1981)
32. Rice, J.R., Ruina, A.L.: Stability of steady frictional slipping. *J. Appl. Mech.* **50**, 343–349 (1983)
33. Ruina, A.L.: Constitutive relations for frictional slip. In: *Mechanics of Geomaterials, Numerical methods in Engineering*, pp 169–187. Wiley, New York (1985)
34. Slemrod, M.: Admissibility criteria for propagating phase boundaries in a van der Waals fluid. *Arch. Ration. Mech. Anal.* **81**, 301–315 (1983)
35. Slepyan, L.I.: The relation between the solutions of mixed dynamical problems for a continuous elastic medium and a lattice. *Sov. Phys. Doklady* **27**(9), 771–772 (1982)
36. Slepyan, L.I., Cherkaev, A., Cherkaev, E.: Transition waves in bistable structures. II. Analytical solution: wave speed and energy dissipation. *J. Mech. Phys. Solids* **53**, 407–436 (2005)
37. Tadmor, E.B., Ortiz, M., Phillips, R.: Quasicontinuum analysis of defects in solids. *Phil. Mag. A* **73**, 1529–1563 (1996)
38. Truskinovsky, L.: Equilibrium interphase boundaries. *Sov. Phys. Doklady* **27**, 306–331 (1982)
39. Truskinovsky, L.: Dynamics of nonequilibrium phase boundaries in a heat conducting elastic medium. *J. Appl. Math. Mech.* **51**, 777–784 (1987)
40. Truskinovsky, L., Vainchtein, A.: Peierls-Nabarro landscape for martensitic phase transitions. *Phys. Rev. B* **67**, 172103 (2003)
41. Truskinovsky, L., Vainchtein, A.: The origin of nucleation peak in transformational plasticity. *J. Mech. Phys. Solids* **52**, 1421–1446 (2004)
42. Truskinovsky, L., Vainchtein, A.: Kinetics of martensitic phase transitions: lattice model. *SIAM J. Appl. Math.* **66**, 533–553 (2005)
43. Truskinovsky, L., Vainchtein, A.: Dynamics of martensitic phase boundaries: discreteness, dissipation and inertia. *Continuum Mech. Thermodyn.* **20**(2), 97–122 (2008)
44. Weiner, J.H.: Dislocation velocities in a linear chain. *Phys. Rev.* **136**(3A), 863–868 (1964)
45. Willis, C.R., El-Batanouny, M., Stancioff, P.: Sine-Gordon kinks on a discrete lattice. I. Hamiltonian formalism. *Phys. Rev. B* **33**, 1904–1911 (1986)